PNAS RESEARCH ARTICLE | APPLIED PHYSICAL SCIENCES OPEN ACCESS

Designing the stripe-ordered cuprate phase diagram through uniaxial-stress

Z. Guguchia[a,1,2], D. Das[a,1], G. Simutis[b,1], T. Adachi[c], J. Küspert[d], N. Kitajima[e], M. Elender[a], V. Grinenko[f], O. Ivashko[g], M. v. Zimmermann[g], M. Müller[h], C. Mielke III[a], F. Hotz[a], C. Mudry[h,i], C. Baines[a], M. Bartkowiak[b], T. Shiroka[a,j], Y. Koike[e], A. Amato[a], C. W. Hicks[k,l], G. D. Gu[m], J. M. Tranquada[m], H.-H. Klauss[n], J. J. Chang[d], M. Janoschek[b,d], and H. Luetkens[a,2]

Edited by J.C. Davis, University of Oxford, Oxford, United Kingdom; received February 28, 2023; accepted November 2, 2023

The ability to efficiently control charge and spin in the cuprate high-temperature superconductors is crucial for fundamental research and underpins technological development. Here, we explore the tunability of magnetism, superconductivity, and crystal structure in the stripe phase of the cuprate $La_{2-x}Ba_xCuO_4$, with $x = 0.115$ and 0.135, by employing temperature-dependent (down to 400 mK) muon-spin rotation and AC susceptibility, as well as X-ray scattering experiments under compressive uniaxial stress in the CuO_2 plane. A sixfold increase of the three-dimensional (3D) superconducting critical temperature T_c and a full recovery of the 3D phase coherence is observed in both samples with the application of extremely low uniaxial stress of ∼0.1 GPa. This finding demonstrates the removal of the well-known 1/8-anomaly of cuprates by uniaxial stress. On the other hand, the spin-stripe order temperature as well as the magnetic fraction at 400 mK show only a modest decrease under stress. Moreover, the onset temperatures of 3D superconductivity and spin-stripe order are very similar in the large stress regime. However, strain produces an inhomogeneous suppression of the spin-stripe order at elevated temperatures. Namely, a substantial decrease of the magnetic volume fraction and a full suppression of the low-temperature tetragonal structure is found under stress, which is a necessary condition for the development of the 3D superconducting phase with optimal T_c. Our results evidence a remarkable cooperation between the long-range static spin-stripe order and the underlying crystalline order with the three-dimensional fully coherent superconductivity. Overall, these results suggest that the stripe- and the SC order may have a common physical mechanism.

cuprate high-temperature superconductor | uniaxial stress | stripe order | superconductivity | muon-spin rotation

Significance

Understanding the degree to which charge-stripe, spin-stripe, and superconducting orders compete/coexist is paramount for elucidating the microscopic pairing mechanism in the cuprate high-temperature superconductors. We explore the tunability of magnetism, superconductivity, and crystal structure in the stripe phase of the cuprate $La_{2-x}Ba_xCuO_4$, by employing complementary techniques under compressive uniaxial stress in the CuO_2 plane. Our results show a sixfold increase of the three-dimensional (3D) superconducting critical temperature T_c with the application of extremely low uniaxial stress of ≃0.1 GPa and evidence a remarkable cooperation between the static spin-stripe order and the underlying crystalline order with the 3D superconductivity. Our results suggest that the underlying pairing mechanisms are essentially the same in the alternative superconducting states with and without spin-stripe order.

High-transition-temperature (high-T_c) superconductivity in copper oxides (cuprates) (1–8) is one of the most intriguing emergent phenomena in strongly correlated electron systems. Besides superconductivity, the phase diagram of some cuprates includes spin- and charge order in patterns of alternating stripes (9–15). There is increasingly strong evidence of static/fluctuating stripe correlations in superconducting cuprates (16–18). One of the most astonishing manifestations of the competition between the various ground states in cuprates occurs in the prototypical cuprate superconductor $La_{2-x}Ba_xCuO_4$ (9–11). It exhibits an anomalous suppression of the uniform three-dimensional (3D) bulk superconductivity when the hole concentration x is near 1/8, where static charge- and spin-stripe orders and a structural phase transition [from a low-temperature orthorhombic (LTO) to a low-temperature-tetragonal (LTT) phase] occur simultaneously (19–21). In the LTT phase, the CuO_6 octahedra rotate about alternate orthogonal axes ([100] and [010]) in successive layers. The atomic displacements in the LTO structure form a diagonal pattern, whereas, in the LTT case, the pattern of displacements is horizontal (or vertical). We note that vertical and diagonal are defined relative to the Cu–O–Cu bond direction. Thus, it is believed that, in the LTT phase, the horizontal stripes are pinned by the lattice potential, which is responsible for the orthogonal stripe order (alternate switching of the stripe direction from plane to plane) along the c axis. While 3D superconductivity is strongly suppressed near $x = 1/8$, 2D superconductivity has the same onset temperature as spin-stripe order (22–24). To explain 2D superconductivity, a pair-density-wave (PDW) order (25, 26) (i.e., spatially modulated SC order) between the charge stripes has been proposed. In this state, the superconducting wave function oscillates from positive to negative from one charge stripe to the next. Because the pinning of the charge stripes by the lattice anisotropy rotates 90° from one layer to the next, the interlayer Josephson coupling is frustrated. While this frustration inhibits the development of 3D superconducting order, it has no restriction on 2D order.

This article is a PNAS Direct Submission.

[1]Z.G., D.D., and G.S. contributed equally to this work.

[2]To whom correspondence may be addressed. Email: zurab.guguchia@psi.ch or hubertus.luetkens@psi.ch.

This article contains supporting information online at https://www.pnas.org/lookup/suppl/doi:10.1073/pnas.2303423120/-/DCSupplemental.

Published December 27, 2023.

Thus, PDW order is considered to be compatible with both the charge and spin-stripe orders. It is believed that uniform d-wave and striped PDW orders are competing SC orders (2, 3). One of the long-standing mysteries in cuprates is whether the stripe- and the superconducting states involve distinct electron-pairing mechanisms and what mechanisms control the competition between such states.

Hydrostatic pressure has long been considered as a way of tuning the stripe phase in cuprates, but it was found that the pressure effect on the 3D superconducting transition temperature in LBCO near 1/8 is quite modest, even with the loss of the long-range LTT structure (27, 28). In-plane uniaxial stress has recently been shown to be a more efficient control parameter (29–37). It was shown that the 2D superconductivity in LBCO (x = 0.115) can be pushed toward 3D order by the application of strain (29). Strain was also shown to affect spin-stripe order in LBCO (x = 0.115). However, the generic character of such observations in a broader region around 1/8 doping is not without ambiguity.

Here, we use in-plane compressive uniaxial stress applied to the CuO_2 layers to perturb the stripe phase of the LBCO phase diagram. An in situ piezoelectrically driven stress device was used to microscopically probe the spin-stripe order with muon spin rotation (μSR) spectroscopy (Fig. 1 *A* and *B*), and the superconducting transitions with ac susceptibility in single crystalline samples of $La_{2-x}Ba_xCuO_4$ with x = 0.115 (below 1/8 doping) and x = 0.135 (above 1/8 doping). The details of the μSR technique, data analysis, and the uniaxial stress devices are published elsewhere (29). The stress effect on the LTO-to-LTT transition in the sample x = 0.115 is probed by X-ray scattering using a recently designed in situ uniaxial pressure

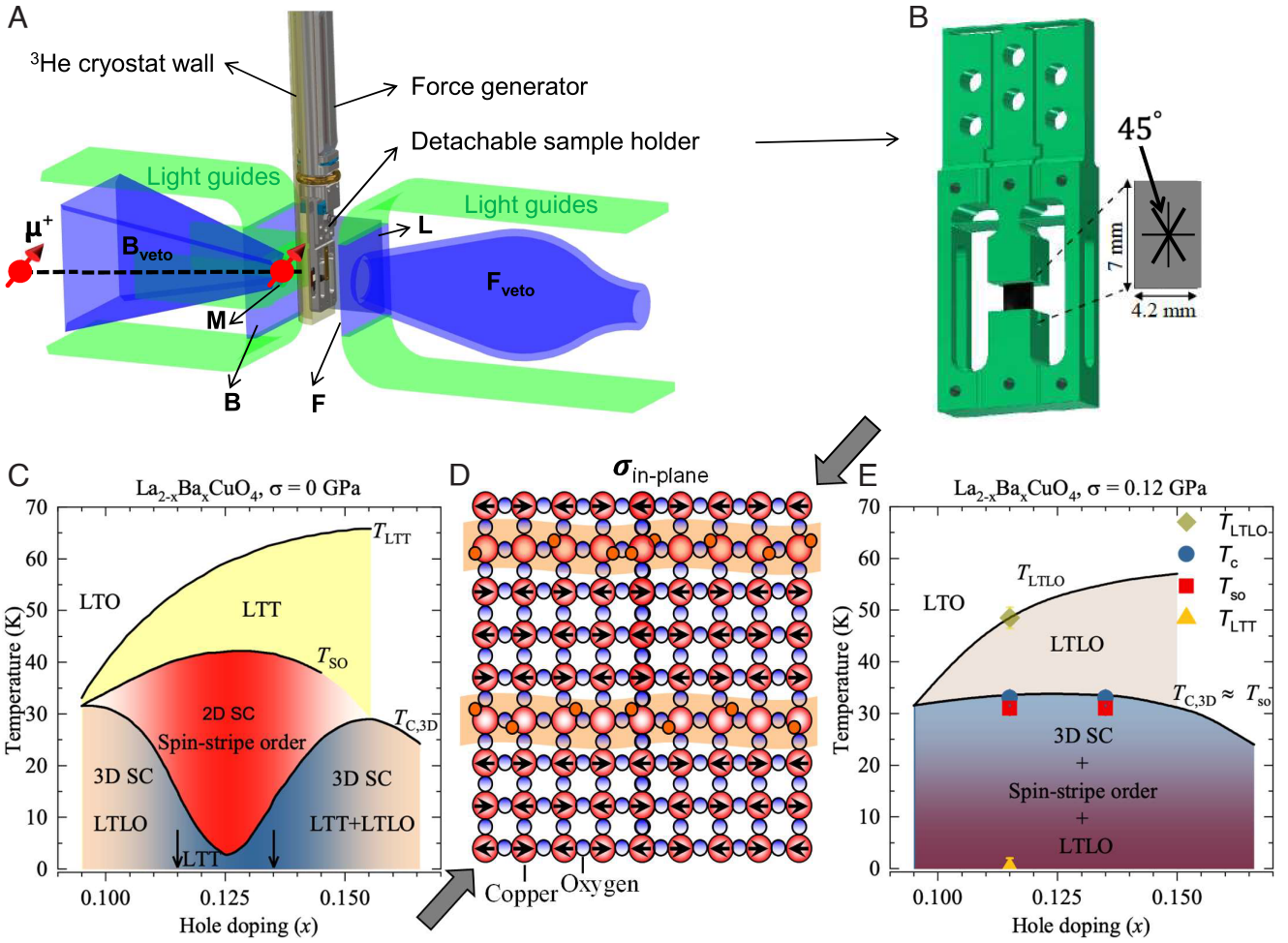

Fig. 1. A schematic overview of the experimental setup and phase diagram. (*A*) A schematic overview of the experimental setup and the uniaxial stress cell. Spin-polarized muons with spin S_μ at 45° with respect to the c-axis of the crystal are implanted in the sample. The sample is surrounded by a backward veto detector B_{veto}, a cup-shaped forward veto detector F_{veto} and four positron detectors: Forward (F), Backward (B), Left (L), and Right (R—not shown for clarity). An electronic clock starts when a muon passes through the muon detector (M) and stops once a decay positron is detected in the positron detectors. B_{veto} consists of a hollow scintillator pyramid with a 7 × 7-mm hole facing the M counter. The purpose of B_{veto} is to collimate the muon beam to a 7 × 7-mm spot and to reject muons (and their decay positrons) missing the aperture. F_{veto} rejects the muons (and their decay positrons) which have not stopped in the sample. (*B*) The uniaxial stress sample holder, used for the μSR experiments. (*C*) The schematic temperature-doping phase diagram of $La_{2-x}Ba_xCuO_4$ for zero-stress σ = 0 GPa. The arrows indicate the present doping values. The various phases in the phase diagram are denoted as follows: Low-temperature orthorhombic (LTO), low-temperature tetragonal (LTT), low-temperature less orthorhombic (LTLO), spin-stripe order (SO), 2D superconductivity (2D SC), and 3D superconductivity (3D SC). (*D*) Illustration of a domain of spin- and charge-stripe order for a layer of LBCO for zero-stress condition (9–11), indicating the periods of the charge ($4a$) and spin ($8a$) modulations. The compressive stress was applied at an angle of 45° to the Cu-O bond direction, as indicated by the gray arrows. (*E*) The conjectured phase diagram of $La_{2-x}Ba_xCuO_4$ at fixed small but not vanishing magnitude strain of σ = 0.12 GPa in the region around x = 1/8 doping. This phase diagram implies that the stress enhances the 3D SC critical temperature $T_{c,3D}$ and reduces slightly the spin-stripe order temperature T_{so} until they acquire similar values $T_{c,3D} \simeq T_{so}$. Stress also causes the reduction of the spin-stripe-ordered volume fraction at elevated temperatures and the full suppression of the LTT phase.

device (32). The details of the sample mounting are given in the *Materials and Methods* section. We show that an extremely low in-plane uniaxial stress of ∼0.1 GPa substantially modifies the temperature-doping phase diagram of LBCO around 1/8-doping (Fig. 1 *C–E*), leading to a phase diagram with no long-range LTT phase (assumed necessary to pin the stripes) and no dip in the 3D T_c, while still preserving the spin-stripe order with $T_{so} \simeq T_{c,3D}$. Since the stress required to establish the phase diagram shown in Fig. 1*C* is very small, we conclude that the spin-stripe order, the spatially modulated 2D (PDW), and uniform 3D SC orders are energetically very finely balanced and that the two SC orders have a similar pairing mechanism.

1. Results

A. Probing Superconductivity under Stress. To monitor the effect of stress on superconductivity in both LBCO-0.115 and LBCO-0.135 (applied at an angle of 45° to the Cu–O bond direction), in situ ac susceptibility measurements were performed. An excitation magnetic field was applied approximately along the *c* axis, either just before or after the μSR measurements, at each stress value. The results are shown in Fig. 2 *A* and *B*. The diamagnetic response of both crystals at 0 GPa corresponds to the measurements before mounting them in the stress apparatus. The samples at zero pressure were zero-field cooled and then measured in a dc field of $\mu_0 H = 0.5$ mT. The field was applied parallel to the CuO_2 planes, so that the resulting shielding currents had to flow between the layers, making the measurement sensitive to the onset of 3D superconductivity below ∼11 K for LBCO-0.115 and below ∼7 K for LBCO-0.135, consistent with previous work (22, 38, 39). The onset of weak diamagnetism near 22 K corresponds to the 2D superconducting order, as it was previously discussed. The superconducting fraction (diamagnetic screening) was estimated to be ∼75 % at $T = 2$K and at ambient conditions. The susceptibility results obtained for the sample outside the stress apparatus were used to calibrate the susceptibility data taken on the sample mounted in the stress apparatus at zero-force condition $\sigma = 0$ GPa. To characterize the changes in the superconducting critical temperature, we identify the onset temperature $T_{c,ons}$ (which equals $T_{c,2D}$ at zero stress) and the midpoint temperature $T_{c,mid}$ (which is a good measure of 3D SC order temperature $T_{c,3D}$), as indicated in Fig. 2 *A* and *B*, and with the strongest diamagnetic response with 100%-volume-fraction superconductivity. Remarkably, the compressive stress causes a rapid rise of $T_{c,mid}$ from 5 to 32 K in LBCO-0.115 and from 3 to 30 K in LBCO-0.135, where $T_{c,mid}$ saturates. The change in $T_{c,ons}$ is much more modest. Namely, $T_{c,ons}$ increases from 20 to 32 K. Consequently, the bulk transition $T_{c,3D}$ of LBCO around 1/8-doping rises from a very suppressed value to the one that is quite similar to the optimal value of SC critical temperature observed in LBCO or LSCO at the same doping level (40). Remarkably, full diamagnetic screening is achieved at low temperatures already at $\sigma = 0.015$ GPa and it stays constant up to the highest applied stress $\sigma = 0.09$ GPa. This observation is different from the case of superoxygenated $La_{2-x}Sr_xCuO_{4+y}$ (41, 42), in which a continuous change of the low-T diamagnetic screening is observed as a function of Sr-content and interpreted as a phase separation between superconducting and magnetic phases.

B. Probing the Spin-Stripe Order under Stress. A combination of weak transverse-field (TF) and zero-field (ZF) μSR measurements were carried out to characterize the evolution of the spin-stripe order with compressive stress using the same device. Measuring the asymmetry between muons counted in detectors on opposite sides of the sample, one obtains the muon spin asymmetry function $A_{TF}(t)$ and $A_{ZF}(t)$, several examples of which are shown in Fig. 3 *A–F*, for TF-μSR and ZF-μSR

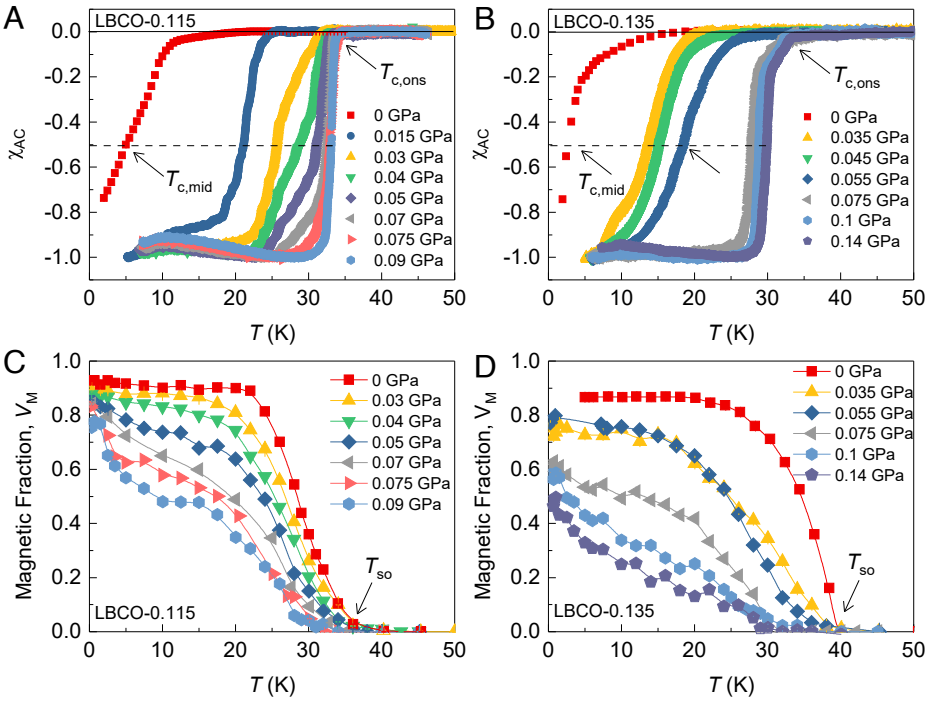

Fig. 2. Superconducting screening and ordered magnetic fraction for LBCO under stress. (*A* and *B*) The temperature dependence of the (dia)magnetic susceptibility for LBCO $x = 0.115$ (*A*) and LBCO $x = 0.135$ (*B*), recorded at ambient and under various degrees of compressive stress. Arrows mark the onset temperature $T_{c,ons}$ and the temperature $T_{c,mid}$ at which $\chi'_{dc} = -0.5$. (*C* and *D*) The temperature dependence of the magnetically ordered volume fraction for LBCO $x = 0.115$ (*C*) and LBCO $x = 0.135$ (*D*) recorded under various stress values.

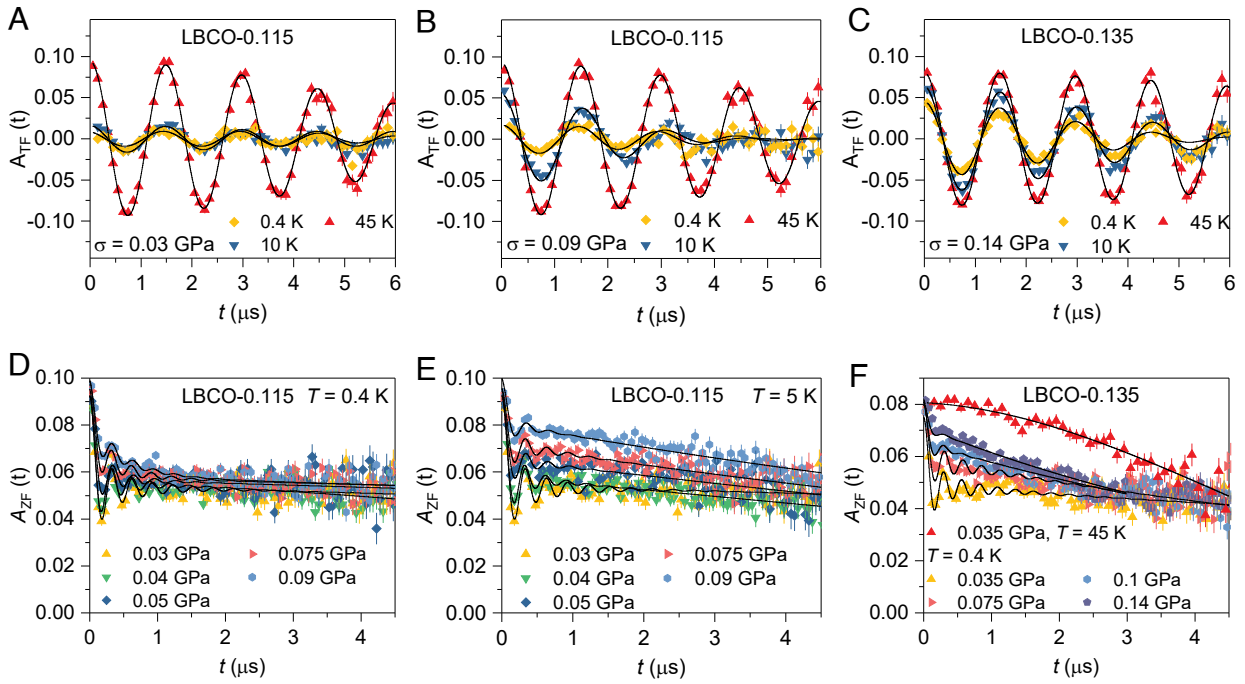

Fig. 3. μSR time spectra for LBCO. Weak-TF μSR spectra for LBCO-0.115, recorded at σ = 0.03 GPa (*A*) and 0.09 GPa (*B*) for various temperatures. (*C*) Weak-TF μSR spectra for LBCO-0.135, recorded at σ = 0.14 GPa for various temperatures. Zero-field μSR spectra for LBCO-0.115, recorded at the base temperature T = 0.4 K (*D*) and at T = 5 K (*E*) under various stress values. (*F*) Zero-field μSR spectra for LBCO-0.135 recorded at T = 0.4 K (i.e., ordered state) under various stress values and at T = 45 K (i.e., paramagnetic state) under 0.035 GPa.

experiments, respectively. In a weak-TF measurement, muons in regions without a local magnetic order precess in the small applied field. Muons that stop in regions with magnetic order and, therefore, experience the vector sum of external and internal fields, dephase rapidly. This causes a rapid reduction in the observable $A_{\rm TF}(0)$ and allows us to determine the magnetically ordered volume fraction $V_{\rm M}$. The maximum amplitude of the weak-TF μSR signal is proportional to the non-magnetic fraction, and the magnetic volume fraction $V_{\rm m}$ can therefore be calculated by $1 - P_{\rm TF}(0)$, where $P_{\rm TF}(t) = A_{\rm TF}(t)/A_{\rm TF}(0)$ is the muon polarization function. At 45 K, $A_{\rm TF}(0)$ has the maximum value and thus $P_{\rm TF}(0) = 1$, indicating that there is no magnetic order. At 0.4 K, both at nearly zero-stress $\sigma = 0.03$ GPa and at the highest applied stress of σ = 0.09 GPa in LBCO-0.115 (Fig. 3*A*), $A_{\rm TF}(0)$ is greatly reduced, indicating the development of magnetic order in most of the sample volume. The temperature dependence of $V_{\rm M}$ for various stress values is presented in Fig. 2 *C* and *D*, for LBCO-0.115 and LBCO-0.135 samples, respectively. Upon increasing stress, there is a decrease in the spin-ordering temperature $T_{\rm so}$, from ~38 K at 0 GPa to ~30 K at 0.09 GPa in both samples. The magnetic volume fraction $V_{\rm M}$ decreases much more steeply, and the effect is stronger in LBCO-0.135 as compared to LBCO-0.115. At 10 K, $V_{\rm M}$ decreases by a factor of two in LBCO-0.115 and by a factor of three in LBCO-0.135, while the diamagnetic screening stays unchanged in the stress region of 0.015–0.09 GPa. Interestingly, the magnetic fraction shows a clear upturn below 10 K, as one can see in Fig. 2 *C* and *D*. In LBCO-0.115 at 0.4 K, $V_{\rm M}$ reaches 80% even at the highest applied stress of 0.09 GPa, which is nearly the same as the one at ambient conditions. These results show that while $V_{\rm M}$ is strongly suppressed at elevated temperatures, it tends to recover below 10 K upon approaching the zero temperature. Therefore, nearly full-volume superconductivity coexists with nearly full volume spin-stripe order in the zero temperature (i.e., quantum) limit in LBCO-0.115. In LBCO-0.135, the magnetic fraction is nearly 50% at T = 0.4 K at the highest applied stress of 0.14 GPa, which coexists with full volume fraction superconductivity.

In ZF-μSR measurements, the muon spins precess exclusively in the internal local field associated with the static long-range magnetic order. As shown in Fig. 3 *D*–*F*, several oscillations remain clearly observable under increasing compressive stress values. This implies that the spin-stripe order remains long-range even at the highest applied stress. We note that the application of stress causes a reduction of the amplitude of ZF-μSR oscillation both for LBCO-0.115 and 0.135, which is partly due to the reduction of the magnetic volume fraction, as seen in TF-μSR experiments. The stress effect is weaker for LBCO-0.115 than for LBCO-0.135. And in LBCO-0.115, the effect at 0.4 K is smaller as compared to 5 K (Fig. 3 *D* and *E*), which is consistent with the TF-μSR measurements. In a single crystal, the amplitude of the oscillation is dependent not only on the magnetically ordered volume fraction $V_{\rm m}$ but also on the angle between the muon spin polarization and the internal field. Since stress may modify the direction of the internal field at the muon stopping site, the change in signal amplitude may partly result from a change of the direction of the internal field. We cannot separate the effect of volume fraction from the effect of field reorientation on the ZF-μSR signal amplitude. Therefore, the weak TF-μSR experiment is a more precise measure of the static magnetically ordered volume fraction.

C. Probing the Crystal Structure under Stress. μSR and AC susceptibility experiments presented above allow us to study the stress effect on superconductivity and spin-stripe order. In order to interpret the results, it is also necessary to characterize the underlying crystalline order (43). To study the uniaxial stress evolution of the structural phase transition from a LTO to a low-temperature tetragonal (LTT) phase, we performed X-ray

scattering experiments at the P21.1 beamline at PETRA-III at DESY in Hamburg, Germany. The crystal was positioned with tetragonal [0,0,1] and [1,1,0] directions spanning the scattering plane and the stress was applied at an angle of 45° to the Cu–O bond direction. Fig. 4*A* shows the high-resolution elastic scattering scans through the $(020)_o/(200)_o$ (refers to orthogonal notation) Bragg peaks at ambient pressure for various temperatures for LBCO-0.115. At 59 K, the LTO peaks are sharp, well separated and have equal intensities, implying equal volume fractions for the respective orthorhombic twin domains. The LTT peak begins to appear below 57 K. Then, there is a coexistence of the LTO and LTT peaks down to approximately 47 K, and below this temperature, a single strong LTT peak is observed. The scans for selected applied stresses are shown in Fig. 4 *B*–*D*. As one can see in Fig. 4*B*, when a stress of 0.017 GPa is applied the intensity of the left LTO peak is suppressed, indicating the structural detwinning of the orthorhombic domains. At this stress value, the appearance of LTT peak is also seen below 54 K. We note that the stress also modifies the scattering angle for the LTT peak, such that it shifts toward the LTO peak. In Fig. 4*E*, we plot the temperature dependence of the integrated intensity of the LTT peak, measured for various uniaxial stresses. To characterize the changes in the structural transition temperatures, we identify the onset temperature $T_{\mathrm{LTT,ons}}$ (below which the LTT phase starts to appear and coexists with the LTO phase) and the temperature T_{LTT} (below which only LTT phase is observed), as indicated in Fig. 4*E*. This plot indicates that at ambient pressure, the onset of the LTO-to-LTT transition is $T_{\mathrm{LTT,ons}} \simeq 57$ K, where the two phases coexist within a 10 K temperature range. For 0.017 GPa, $T_{\mathrm{LTT,ons}}$ is slightly reduced and there is a broader temperature region of coexistence. When stress is increased to 0.033 GPa, the onset of the LTT–LTO transition remains nearly unchanged, the coexistence region is further broadened and the LTT peak shifts further toward the LTO peak. As one can see in Fig. 4*C*, upon increasing the stress to 0.06 GPa, a sharp LTO peak is observed from 54 K down to 45 K. Then, upon further lowering the temperature, there is no development of an LTT peak. If the system would exhibit a LTO phase down to the base-T the peak position and the intensity should stay constant with

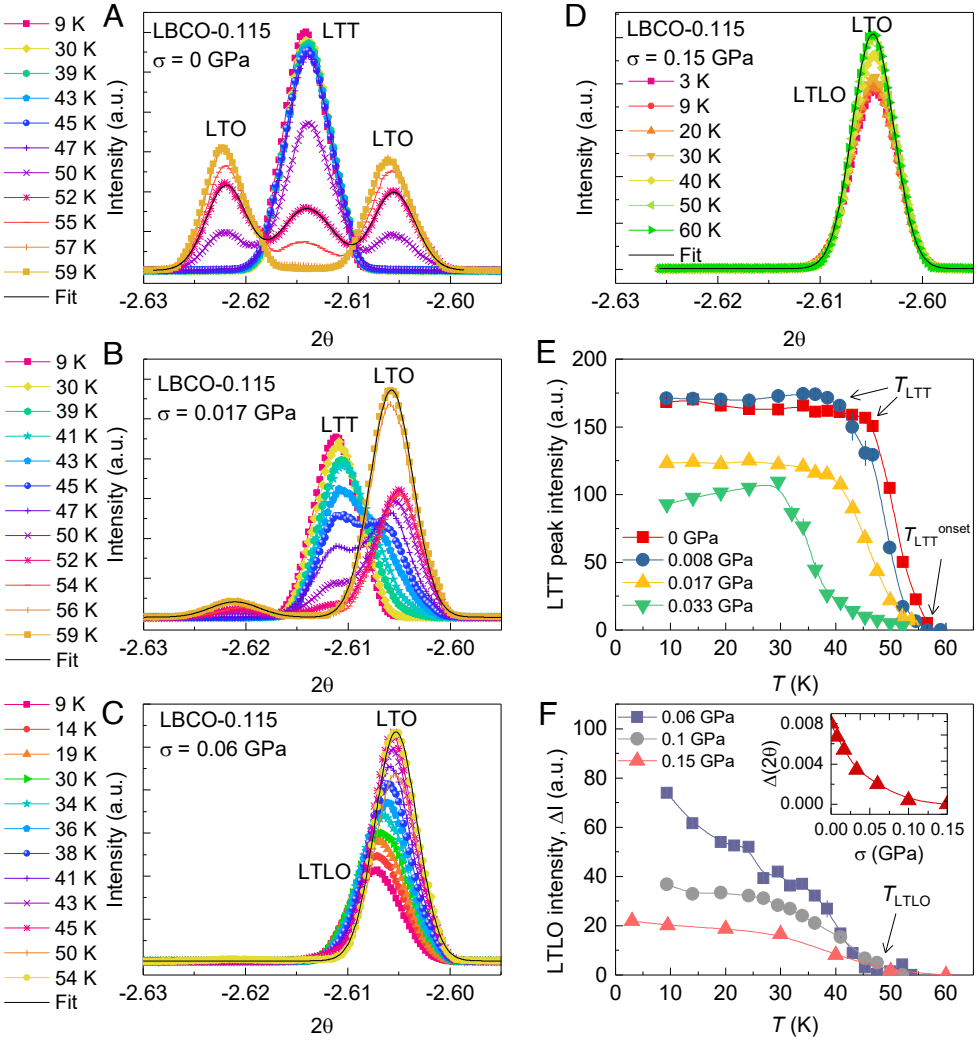

Fig. 4. (*A*) Structural transition in LBCO under uniaxial stress. Scans of the $(020)_o/(200)_o$ Bragg reflections at several temperatures through the transition from the LTO phase to the LTT phase, measured under an uniaxial stress of 0 GPa (*A*), 0.017 GPa (*B*), 0.06 GPa (*C*), and 0.15 GPa (*D*). (*E*) The temperature dependences of the LTT integrated peak intensities for LBCO-0.115, measured under various stress values up to 0.033 GPa. Black solid lines in panels (*A*–*D*) represent the fits of the data using multi- or single-component Gaussian functions. (*F*) The temperature dependence of the intensity $\Delta I(T) = I(T > 50\ \mathrm{K}) - I(T)$, which is interpreted as the intensity of the LTLO phase (phase with reduced orthorhombicity), for LBCO-0.115, measured under various stress values above 0.033 GPa. The inset shows the difference between the scattering angle measured at $T > 50$ K and that at base-T of 9 K, i.e., $\Delta(2\theta) = 2\theta(T > 50\ \mathrm{K}) - 2\theta(T = 9\ \mathrm{K})$.

temperature. Instead, the intensity of the LTO peak decreases and it shifts slightly toward higher scattering angles. We interpret this behavior as the occurrence of an intervening LTLO phase and the intensity variation can be understood as a reduction in orthorhombicity. Thus, the scattering intensity seems to provide a precise measure of the LTO-LTLO structural change. The temperature dependence of the intensity $\Delta I(T) = I(T > 50\ \text{K}) - I(T)$, which is interpreted as the intensity of the LTLO phase (phase with reduced orthorhombicity), for LBCO-0.115, measured under various stress values above 0.033 GPa are shown in Fig. 4*F*. Here, the *Inset* shows the difference between the scattering angle measured at $T > 50$ K and that at base-T of 9 K, i.e., $\Delta(2\theta) = 2\theta(T > 50\ \text{K}) - 2\theta(T = 9\ \text{K})$. When applying stresses higher than 0.06 GPa the LTO peak intensity and the scattering angle are less affected and show only a weak temperature dependence, as shown in Fig. 4 *D* and *F*. These results suggest that, at low temperatures, the stress tends to stabilize the full volume LTLO phase.

Even at a low level of stress, as in Fig. 4*B*, one can see that one set of LTO twin domains is substantially suppressed. The peak labeled LTT is also shifted with respect to the zero-stress measurement in Fig. 4*A*. It is reasonable to expect that finite stress changes the symmetry from LTT to LTLO; we see a shift rather than a splitting of the LTT/LTLO peak because the orthogonal twin domains are depressed and the signal is not resolved. From this perspective, the low-temperature structure may be LTLO for all measurements with finite stress, with the orthorhombic strain increasing continuously with the applied stress.

D. Phase Diagram. Our overall results are summarized in Fig. 5. The spin-stripe order temperature T_{so}, the LTO-to-LTT/LTLO structural phase transition temperature, and superconducting transition temperatures are plotted against stress in Fig. 5 *A* and *B* for LBCO-0.115 and LBCO-0.135, respectively. The stress dependence of the low-temperature value of magnetic volume fraction and internal magnetic field at 0.4 K are shown in Fig. 5 *C* and *D*. Fig. 5 *A* and *B* show that the crossover from 2D to 3D superconducting order occurs at a characteristic critical uniaxial stress of σ_{cr} = 0.06 GPa for LBCO-0.115 and 0.08 GPa for LBCO-0.135. Remarkably, establishment of optimal 3D SC order is followed by the full suppression of the LTT structure at σ_{cr} = 0.06 GPa, which is replaced by the LTLO structure,

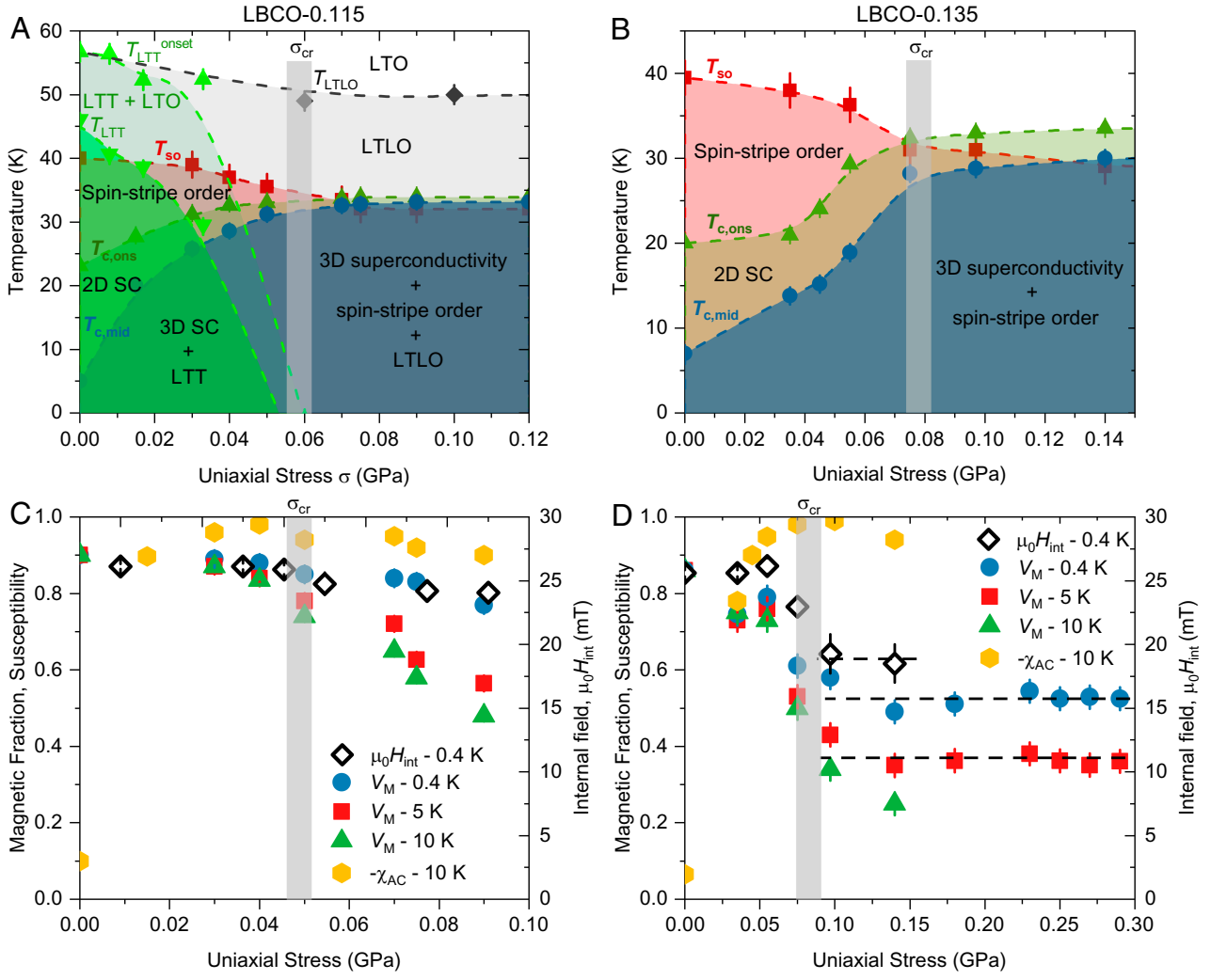

Fig. 5. (*A*) Phase diagrams of LBCO under uniaxial stress. Dependence of the SC transition temperatures ($T_{c,2D}$, $T_{c,3D}$) and of static spin-stripe order temperature (T_{so}) on compressive stress in LBCO $x = 0.115$ (*A*) and in LBCO $x = 0.135$ (*B*). The stress dependence of the structural transition temperatures (T_{LTT}, T_{LTO}) for LBCO $x = 0.115$ is also shown in panel (*A*). The black arrow marks the critical stress value σ_{cr}, above which a sharp 3D SC transition is established. (*C* and *D*) The stress dependence of the internal magnetic field B_{int} for the base-T of 0.4 K, of the diamagnetic susceptibility χ_{AC} for T = 10 K and of magnetically ordered fraction V_M for various temperatures T = 0.4 K, 5 K, and 10 K for LBCO $x = 0.115$ (*C*) and LBCO $x = 0.135$ (*D*). Vertical gray lines mark the critical stress value σ_{cr}.

as it was demonstrated for the $x = 0.115$ sample. Interestingly, T_{so} decreases by small amount to essentially match $T_{c,mid}$ for $\sigma > \sigma_{cr}$ for both samples. We note that, only a modest stress-induced decrease in B_{int} (Fig. 5 *C* and *D*) is resolved, indicating that the magnetic structure is well ordered also under stress. The dominant change of the spin-stripe order induced by uniaxial stress is a strong reduction in V_M at elevated temperatures. V_M decreases upon approaching the critical stress value σ_{cr}, reaches the minimum value just above σ_{cr} and then stays constant. The stress effect on V_M is stronger in LBCO-0.135 as compared to LBCO-0.115. We note that the stress effect at 400 mK is largely reduced as compared to 10 K, where V_M shows strong stress-induced suppression. This shows that in the zero-temperature limit, the large-volume-fraction spin-stripe order is compatible with 3D superconducting order. But it seems that the reduction of magnetic fraction and the suppression of the LTT structure is a necessary condition to establish 3D superconducting coherence with optimal T_c.

2. Discussion

Our experiments show that when a LBCO sample exhibits a nearly 100% spin-stripe order V_M and a long-range LTT structure, it also exhibits 2D superconductivity and a strongly depressed 3D SC transition. As V_M decreases and the LTT structure is suppressed, the 3D SC transition temperature rises. To interpret these results, we first recall that around $x = 1/8$, there is a structural phase transition from LTO to an LTT phase. The LTT structure favors the orthogonal stripe order in alternating layers along the *c* axis. A finite interlayer Josephson coupling would normally be expected to lock the phases of the superconducting wave function between the layers, resulting in 3D SC order. To explain the apparent frustration of such interlayer Josephson coupling, pair-density-wave order within the layers has been proposed (4, 25, 26), which is compatible with both the charge- and spin-stripe orders. Such an anti-phase SC order combined with the LTT structure and the orthogonal stripe ordering could explain the frustrated Josephson coupling between the layers and the suppression of bulk 3D SC order, while the 2D SC correlations within the CuO_2 layers still coexist with the static spin-stripe order. The suppression of the tetragonal structure under applied stress implies that stress disfavors an orthogonal stripe arrangement and lifts the geometric frustration. As a result, the ordered fraction V_M of spin-stripe order is partly reduced, which seems sufficient to let the system establish 3D superconductivity and to enormously enhance its SC critical temperature. A reduction of the magnetic fraction V_M under stress is expected to promote patches of uniform *d*-wave superconductivity. Patches in adjacent layers whose projections overlap, mediate a non-zero interlayer coupling. However, as long as such patches are sparse, the PDW of the stripes dominates the intralayer physics, and the interlayer couplings are thus frustrated. Beyond a critical patch fraction, the superconducting phase is expected to develop uniform long-range order, with a defined phase relationship between the majority of patches. At this point, one expects $T_{c,3D}$ to coincide with $T_{c,2D}$. The idea of intermixed regions of PDW and uniform d-wave SC order is a plausible concept that must be considered. A straightforward theoretical prediction is that if PDW and spatially uniform superconductivity coexist, then there should be an induced CDW with a period that is equal to that of the PDW (44). In terms of the modulation wave vector, if one writes the wave vector for charge stripes as 2Q, then the induced CDW peak should be at 1Q. The only case where the 1Q peak has been detected is in vortex halos measured in Bi2212 by STM (45) and the signal was only present within a certain range of bias voltage. The absence of such evidence in other cuprates has been a concern (46); however, a new study reports evidence of a 1Q peak detected by resonant soft x-ray scattering in Fe-doped $La_{1.87}Sr_{0.13}CuO_4$ and Sr-doped LBCO $x = 0.125$ (47).

We note that superoxygenated $La_{2-x}Sr_xCuO_{4+y}$ (41, 42, 48) shows similar superconducting and magnetic transition temperatures (15), which is also the case for LBCO samples investigated here ($x = 0.115$ and $x = 0.135$) above the critical stress. However, there is one important difference between LBCO under stress and the superoxygenated $La_{2-x}Sr_xCuO_{4+y}$. In $La_{2-x}Sr_xCuO_{4+y}$, superconducting fraction (diamagnetic screening) changes with Sr concentration and the reduction of superconducting fraction is correlated with the increase of the magnetic fraction. So, there is a negative linear correlation between the magnetic and superconducting fractions in superoxygenated $La_{2-x}Sr_xCuO_{4+y}$, which implies phase separation (41). By contrast, in the LBCO-0.115 and LBCO-0.135 samples under stress, we do not observe a negative linear correlation between the magnetic and superconducting fractions. The superconducting fraction (diamagnetic screening) becomes large within the stress region of $\sigma \simeq 0.01$–0.02 GPa and stays unchanged up to the maximum applied stress. The fraction of the spin-stripe ordered state decreases under stress, but a substantial fraction of the sample remains magnetic even in the presence of large volume fraction 3D superconductivity.

In conclusion, we used muon spin rotation, magnetic susceptibility, and X-ray scattering experiments to follow the evolution of the spin-stripe order, superconductivity, and LTO-LTT structural phase transition in LBCO with $x = 0.115$ and $x = 0.135$ as a function of stress applied within the CuO_2 planes (at an angle of 45° to the Cu-O bond direction). Stress induces a full suppression of the LTT structural phase and substantial decrease in the magnetic volume fraction at elevated temperatures, as well as a dramatic rise in the onset of 3D superconductivity on both sides of 1/8 anomaly in the phase diagram. However, the spin-stripe order temperature, as well as the magnetic fraction at 400 mK shows only a modest decrease under stress. Moreover, the onset temperature for the 3D superconductivity and the spin-stripe order are quite similar in the less frustrated large stress regime (beyond the critical stress $\sigma_{cr} \sim 0.06$ GPa), from which we infer that the same kind of electronic interactions are responsible for both phenomena (18). Our data demonstrate that in-plane strain can be used to affect the phase competition in the striped cuprates. Namely, by strain tuning the magnetic fraction and the crystal structure, one can switch between anti-phase PDW and uniform *d*-wave SC orders. Our results raise fundamental theoretical questions concerning the nature of the strain-stimulated cooperation between the 3D SC and the magnetic order in the stripe phase of cuprates and might shed light on the high-T_c problem.

3. Materials and Methods

Sample Preparation. Polycrystalline samples of $La_{2-x}Ba_xCuO_4$ with $x = 0.115$ and $x = 0.135$ were prepared by the conventional solid-state reaction method using La_2O_3, $BaCO_3$, and CuO as starting materials. The single-phase character of the samples was checked by powder X-ray diffraction. The single crystals of $La_{2-x}Ba_xCuO_4$ with $x = 0.115$ and $x = 0.135$ were grown by the traveling solvent floating-zone method (39). All the measurements were performed on samples from the same batch.

Uniaxial strain devices. For the μSR and AC susceptibility measurements, we used the piezoelectric-driven uniaxial pressure apparatus (29, 49, 50) designed for operation at cryogenic temperatures, where the sample geometry and sample size are suitable for muon spin rotation and relaxation experiments. The apparatus fits into the *Oxford Heliox* ^{3}He cryostat of the general purpose instrument Dolly on the πE1 beamline at the Paul Scherrer Institute. The use of piezoelectric actuators allows for a continuous in situ tunability of the applied pressure. The sample is mounted in a detachable holder, made of titanium that allows rapid sample exchange, as described in detail in our previous work (29). The holder incorporates two pairs of flexures that protect the sample against inadvertent torques and transverse forces. The space around the sample is kept as open as possible, so that muons that miss the sample pass through the holder and are picked up by the veto counter (the purpose of veto counter is to reject muons and their decay positrons that have missed the sample). The sample plates were masked with hematite foils, which strongly depolarizes the incoming muons resulting in loss of asymmetry (signal). We managed to have around $\sim$40% of the incoming muons stopped in the sample. The sample holder was attached to the main part of the apparatus, which is called the strain generator, and which contains the piezoelectric actuators.

We used a $La_{1.885}Ba_{0.115}CuO_4$ and $La_{1.865}Ba_{0.135}CuO_4$ samples (referred to as LBCO-0.115 and LBCO-0.135 in the following) (7 mm $\times$ 4 mm $\times$ 0.6 mm) oriented along a crystallographic direction which is off by 45° from the *a* axis. The sample was fixed on the sample holder by using epoxy (Stycast-2850 FT) and mounted on a sample holder consisting of grade-2 Ti. A pair of coils (each having 100 turns) was placed very close to the sample for in situ ac-susceptibility (ACS) measurements (29). These allowed us to determine the T_c of LBCO-0.115 and LBCO-0.135 under different stress conditions. The area facing the muon beam was 4×4.2 mm^2.

The samples were cooled down while keeping the piezoelectric actuators grounded. We applied the compressive stress at 45 K, followed by a system cooling down to 0.4 K. ACS and μSR measurements were carried out upon warming the sample. In order to apply a compressive stress to the sample, a positive voltage was applied in the compression stack (V_C). To avoid possible electrical discharges of He gas at 45 K, we had to limit V_C to +100 V. To achieve a higher compressive force, we kept $V_C = +100$ V and applied a negative voltage in the tension stack (V_T).

For the X-ray experiments, the uniaxial pressure was generated using a dedicated sample stick with a linear actuator generating the force. Integrated feedback mechanisms ensured a constant applied pressure during the temperature scans as described elsewhere (32). X-ray scattering experiments were carried out at the P21.1 beamline at PETRA-III. The crystal was positioned with the tetragonal [0,0,1] and [1,1,0] directions spanning the scattering plane and the stress was applied at an angle of 45° to the Cu-O bond direction. A single bent-Laue Si monochromator on the (311) reflection was used, resulting in an energy of 101.6 keV. The monochromator crystal was bent toward the sample, increasing the effective incident flux. Scattering from the sample was filtered with a perfect Si analyzer using the (311) reflection in Laue geometry. The resulting scattered light was collected by a PILATUSX CdTe 100k pixel detector, and the intensity was integrated over a region of interest.

Principles of the μSR technique and the data analysis. Detailed information on μSR technique (51–53) and for the procedure of data analysis is described in *SI Appendix*.

Data, Materials, and Software Availability. All study data are included in the article and/or *SI Appendix*.

ACKNOWLEDGMENTS. Muon spin rotation experiments were performed at the Swiss Muon Source SμS, Paul Scherrer Institute, Villigen, Switzerland. Z.G. acknowledges support from the Swiss National Science Foundation (SNSF) through SNSF Starting Grant (No. TMSGI2_211750). C.W.H. acknowledges the support of the Max Planck Society and the German Research Foundation (TRR288-422213477 ELASTO-Q-MAT, Project A10). We acknowledge Deutsches Elektronen-Synchrotron (Hamburg, Germany), a member of the Helmholtz Association, for the provision of experimental facilities. Parts of this research were carried out at PETRA III, and we would like to thank Philipp Glaevecke and Olof Gutowski for assistance in using P21.1. Beamtime was allocated for proposal I-20210503 EC. Work at Brookhaven is supported by the Office of Basic Energy Sciences, Materials Sciences and Engineering Division, U.S. Department of Energy under Contract No. DE-SC0012704. We acknowledge Prof. Yasmine Sassa for useful discussions. M.M. acknowledges financial support from the Swiss National Science Foundation under grant No. 200020_200558. H.-H.K. acknowledges support from the German Science Foundation (DFG) grant No. SFB1143.

Author affiliations: [a]Laboratory for Muon Spin Spectroscopy, Paul Scherrer Institute, CH-5232 Villigen, Switzerland; [b]Laboratory for Neutron and Muon Instrumentation, Paul Scherrer Institut, CH-5232 Villigen, Switzerland; [c]Department of Engineering and Applied Sciences, Sophia University, Tokyo 102-8554, Japan; [d]Physik-Institut, Universität Zürich, CH-8057 Zürich, Switzerland; [e]Department of Applied Physics, Tohoku University, Sendai 980-8579, Japan; [f]Tsung-Dao Lee Institute, Shanghai Jiao Tong University, Pudong, 201210 Shanghai, China; [g]Deutsches Elektronen-Synchrotron, 22607 Hamburg, Germany; [h]Condensed Matter Theory Group, Paul Scherrer Institute, CH-5232 Villigen, Switzerland; [i]Institut de Physique, École Polytechnique Fédérale de Lausanne, Lausanne CH-1015, Switzerland; [j]Laboratorium für Festkörperphysik, ETH Zürich, CH-8093 Zürich, Switzerland; [k]Max Planck Institute for Chemical Physics of Solids, D-01187 Dresden, Germany; [l]School of Physics and Astronomy, University of Birmingham, Birmingham B15 2TT, United Kingdom; [m]Condensed Matter Physics and Materials Science Division, Brookhaven National Laboratory, Upton, NY 11973; and [n]Institute for Solid State and Materials Physics, Technische Universitat Dresden, D-01069 Dresden, Germany

Author contributions: Z.G. designed research; Z.G., D.D., G.S., T.A., J.K., N.K., M.E., V.G., O.I., M.v.Z., M.M., C. Mielke, F.H., C. Mudry, C.B., M.B., T.S., Y.K., A.A., C.W.H., G.D.G., J.M.T., H.-H.K., J.J.C., M.J., and H.L. performed research; Z.G. analyzed data; and Z.G. wrote the paper with feedback from all authors.

The authors declare no competing interest.

1. J. G. Bednorz, K. A. Müller, Possible high T_c superconductivity in the Ba–La–Cu–O system. *Z. Phys. B* **64**, 189 (1986).
2. N. J. Robinson, P. D. Johnson, T. M. Rice, A. M. Tsvelik, Anomalies in the pseudogap phase of the cuprates: Competing ground states and the role of umklapp scattering. *Rep. Prog. Phys.* **82**, 126501 (2019).
3. D. F. Agterberg *et al.*, The physics of pair density waves. *Annu. Rev. Condens. Matter Phys.* **11**, 231 (2019).
4. E. Berg *et al.*, Dynamical layer decoupling in a stripe-ordered high-T_c superconductor. *Phys. Rev. Lett.* **99**, 127003 (2007).
5. Q. Li, M. Hücker, G. D. Gu, A. M. Tsvelik, J. M. Tranquada, Two-dimensional superconducting fluctuations in stripe-ordered $La_{1.875}Ba_{0.125}CuO_4$. *Phys. Rev. Lett.* **99**, 067001 (2007).
6. A. Abanov, A. V. Chubukov, J. Schmalian, Fingerprints of spin mediated pairing in cuprates. *J. Electron Spectrosc. Relat. Phenom.* **117**, 129, strongly correlated systems (2001).
7. I. Vekhter, C. M. Varma, Proposal to determine the spectrum of pairing glue in high-temperature superconductors. *Phys. Rev. Lett.* **90**, 237003 (2003).
8. T. Dahm *et al.*, Strength of the spin-fluctuation-mediated pairing interaction in a high-temperature superconductor. *Nat. Phys.* **5**, 217 (2009).
9. J. M. Tranquada, B. J. Sternlieb, J. D. Axe, Y. Nakamura, S. Uchida, Evidence for stripe correlations of spins and holes in copper oxide superconductors. *Nature (London)* **375**, 561 (1995).
10. M. Hücker *et al.*, Stripe order in superconducting $La_{2-x}Ba_xCuO_4$ ($0.095 \leq x \leq 0.155$). *Phys. Rev. B.* **83**, 104506 (2011).
11. J. M. Tranquada *et al.*, Neutron-scattering study of stripe-phase order of holes and spins in $La_{1.48}Nd_{0.4}Sr_{0.12}CuO_4$. *Phys. Rev. B* **54**, 7489 (1996).
12. P. Abbamonte *et al.*, Spatially modulated "Mottness" in $La_{2-x}Ba_xCuO_4$. *Nat. Phys.* **1**, 155 (2005).
13. M. Vojta, Lattice symmetry breaking in cuprate superconductors: Stripes, nematics, and superconductivity. *Adv. Phys.* **58**, 699 (2009).
14. S. A. Kivelson *et al.*, How to detect fluctuating stripes in the high-temperature superconductors. *Rev. Mod. Phys.* **75**, 1201 (2003).
15. S. A. Kivelson, G. Aeppli, V. J. Emery, Thermodynamics of the interplay between magnetism and high-temperature superconductivity. *Proc. Natl. Acad. Sci. U.S.A.* **98**, 11903–11907 (2001).
16. T. Wu *et al.*, Magnetic-field-induced charge-stripe order in the high-temperature superconductor $YBa_2Cu_3O_y$. *Nature* **477**, 191–194 (2011).
17. J. Chang *et al.*, Direct observation of competition between superconductivity and charge density wave order in $YBa_2Cu_3O_{6.67}$. *Nat. Phys.* **8**, 871–876 (2012).
18. J. M. Tranquada, Cuprate superconductors as viewed through a striped lens. *Adv. Phys.* **69**, 437–509 (2020).
19. J. D. Axe, M. K. Crawford, Structural instabilities in lanthanum cuprate superconductors. *J. Low Temp. Phys.* **95**, 271 (1994).
20. H. H. Klauss, Spin stripe order and superconductivity in layered transition metal oxides. *JPCM* **16**, S4457–S4478 (2004).
21. H. H. Klauss, From antiferromagnetic order to static magnetic stripes: The phase diagram of $(La, Eu)_{2-x}Sr_xCuO_4$. *Phys. Rev. Lett.* **85**, 4590 (2000).
22. J. M. Tranquada *et al.*, Evidence for unusual superconducting correlations coexisting with stripe order in $La_{1.875}Ba_{0.125}CuO_4$. *Phys. Rev. B* **78**, 174529 (2008).
23. Q. Li *et al.*, Two-dimensional superconducting fluctuations in stripe-ordered $La_{1.875}Ba_{0.125}CuO_4$. *Phys. Rev. Lett.* **99**, 067001 (2007).

24. Z. Guguchia *et al*., Cooperative coupling of static magnetism and bulk superconductivity in the stripe phase of $La_{2-x}Ba_xCuO_4$: Pressure ($x = 0.155, 0.17$) and doping ($x = 0.11$–0.17) dependent studies. *Phys. Rev. B* **94**, 214511 (2016).
25. E. Fradkin, S. A. Kivelson, J. M. Tranquada, Colloquium: Theory of intertwined orders in high temperature superconductors. *Rev. Mod. Phys.* **87**, 457 (2015).
26. A. Himeda, T. Kato, M. Ogata, Stripe states with spatially oscillating *d*-wave superconductivity in the two-dimensional t–J model. *Phys. Rev. Lett.* **88**, 117001 (2002).
27. M. Hücker *et al*., Spontaneous symmetry breaking by charge stripes in the high pressure phase of superconducting $La_{1.875}Ba_{0.125}CuO_4$. *Phys. Rev. Lett.* **104**, 057004 (2010).
28. Z. Guguchia *et al*., Tuning the static spin-stripe phase and superconductivity in $La_{2-x}Ba_xCuO_4$ ($x = 1/8$) by hydrostatic pressure. *New J. Phys.* **15**, 093005 (2013).
29. Z. Guguchia *et al*., Using uniaxial stress to probe the relationship between competing superconducting states in a cuprate with spin-stripe order. *Phys. Rev. Lett.* **125**, 097005 (2020).
30. M. Fujita *et al*., Stripe order, depinning, and fluctuations in $La_{1.875}Ba_{0.125}CuO_4$ and $La_{1.875}Ba_{0.075}Sr_{0.05}CuO_4$. *Phys. Rev. B* **70**, 104517 (2004).
31. T. J. Boyle *et al*., Large response of charge stripes to uniaxial stress in $La_{1.475}Nd_{0.4}Sr_{0.125}CuO_4$. *Phys. Rev. Res.* **3**, L022004 (2021).
32. G. Simutis *et al*., In-situ uniaxial pressure cell for X-ray and neutron scattering experiments. *Rev. Sci. Inst.* **94**, 013906 (2023).
33. G. Simutis *et al*., Single domain stripe order in a high-temperature superconductor. *Commun. Phys.* **5**, 296 (2022).
34. J. Choi *et al*., Disentangling intertwined quantum states in a prototypical cuprate superconductor. *Phys. Rev. Lett.* **128**, 207002 (2022).
35. Q. Wang *et al*., Uniaxial pressure induced stripe order rotation in $La_{1.88}Sr_{0.12}CuO_4$. *Nat. Commun.* **13**, 1795 (2022).
36. H.-H. Kim *et al*., Uniaxial pressure control of competing orders in a high-temperature superconductor. *Science* **362**, 1040 (2018).
37. M. E. Kamminga *et al*., Evolution of magnetic stripes under uniaxial stress in $La_{1.885}Ba_{0.115}CuO_4$ studied by neutron scattering. *Phys. Rev. B* **107**, 144506 (2023).
38. Z. Guguchia *et al*., Complementary response of static spin-stripe order and superconductivity to non-magnetic impurities in cuprates. *Phys. Rev. Lett.* **119**, 087002 (2017).
39. T. Adachi *et al*., Crystal growth, transport properties, and crystal structure of the single-crystal $La_{1.885}Ba_{0.115}CuO_4$. *Phys. Rev. B* **64**, 144524 (2001).
40. H. Takagi *et al*., Superconductor-to-nonsuperconductor transition in $(La_{1-x}Sr_x)_2CuO_4$ as investigated by transport and magnetic measurements. *Phys. Rev. B* **40**, 2254 (1989).
41. H. E. Mohottala *et al*., Phase separation in superoxygenated $La_{2-x}Sr_xCuO_{4+y}$. *Nat. Mater.* **5**, 377 (2006).
42. L. Udby *et al*., Measurement of unique magnetic and superconducting phases in oxygen-doped high-temperature superconductors $La_{2-x}Sr_xCuO_{4+y}$. *Phys. Rev. Lett.* **111**, 227001 (2013).
43. R. Frison *et al*., Crystal symmetry of stripe-ordered $La_{1.88}Sr_{0.12}CuO_4$. *Phys. Rev. B* **105**, 224113 (2022).
44. E. Berg, E. Fradkin, S. A. Kivelson, J. M. Tranquada, Striped superconductors: How spin, charge and superconducting orders intertwine in the cuprates. *New J. Phys.* **11**, 115004 (2009).
45. S. D. Edkins *et al*., Magnetic field-induced pair density wave state in the cuprate vortex halo. *Science* **364**, 976–980 (2019).
46. E. Blackburn *et al*., Searching for the signature of a pair density wave in $YBa_2Cu_3O_{6.67}$ using high energy X-ray diffraction. arXiv [Prerpint] (2023). http://arxiv.org/abs/2310.18302 (Accessed 27 October 2023).
47. J.-S. Lee *et al*., Pair-density wave signature observed by X-ray scattering in La-based high-T_c cuprates. arXiv [Preprint] (2023). http://arxiv.org/abs/2310.19907 (Accessed 30 October 2023).
48. A.-E. Tutueanu *et al*., Nature of the magnetic stripes in fully oxygenated La_2CuO_{4+y}. *Phys. Rev. B* **103**, 045138 (2021).
49. C. W. Hicks, S. Ghosh, M. E. Barber, H.-H. Klauss, Piezoelectric-driven uniaxial stress apparatus for muon spin rotation. *JPS Conf. Proc.* **21**, 011040 (2018).
50. V. Grinenko *et al*., Split superconducting and time-reversal symmetry-breaking transitions in Sr_2RuO_4 under stress. *Nat. Phys.* **17**, 748–754 (2021).
51. P. Dalmas de Reotier, A. Yaouanc, Muon spin rotation and relaxation in magnetic materials. *J. Phys.: Condens. Matter* **9**, 9113–9166 (1997).
52. B. Nachumi *et al*., Muon spin relaxation study of the stripe phase order in $La_{1.6-x}Nd_{0.4}Sr_xCuO_4$ and related 214 cuprates. *Phys. Rev. B* **58**, 8760–8772 (1998).
53. A. Suter, B. M. Wojek, Musrfit: A free platform-independent framework for μSR data analysis. *Phys. Procedia* **30**, 69–73 (2012).